# Electronic Supplementary Material (ESI) for

# An effective integrated design for enhanced cathodes of Ni foam supported Pt/CNTs for Li-$O_2$ batteries

*Jiaxin Li*[§†], *Yi Zhao*[§], *Mingzhong Zou*[†], *ChuXin Wu*[§], *Zhigao Huang*[†*], *Lunhui Guan*[§#*]

[§]State Key Laboratory of Structural Chemistry Fujian Institute of Research on the Structure of Matter, Chinese Academy of Sciences, Fuzhou 350002, China

[†]College of Physics and Energy, Fujian Normal University, Fuzhou, 350007, China

[#]Key Laboratory of Design and Assembly of Functional Nanostructures, Chinese Academy of Sciences， Fuzhou 350002, China

*Telephone/Fax: 86-591-83792835. E-mail: guanlh@fjirsm.ac.cn, zghuang@fjnu.edu.cn.

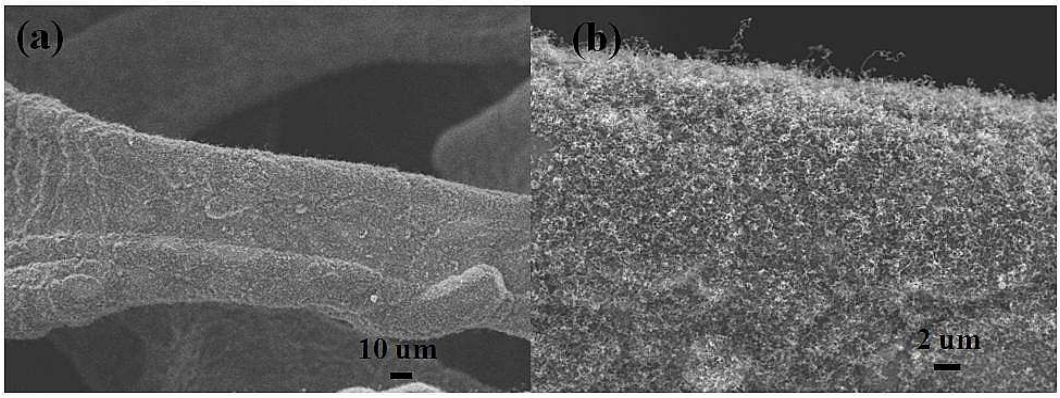


**Figure S1.** (a) SEM image and (b) magnified SEM image of Pt/CNTs-NF.

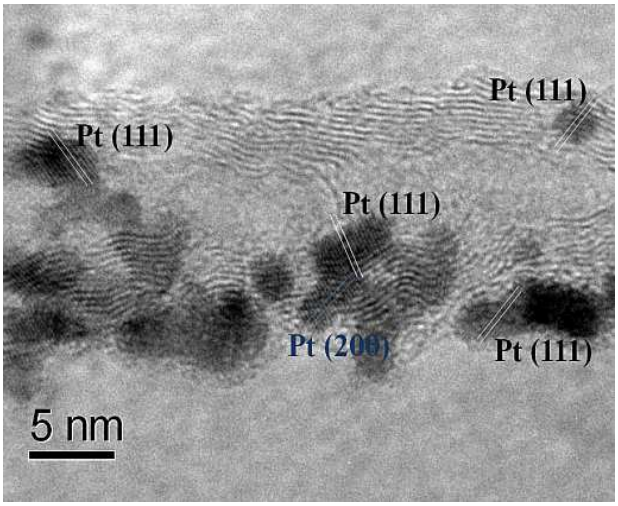


**Figure S2.** HR-TEM image of Pt/CNTs-NF.

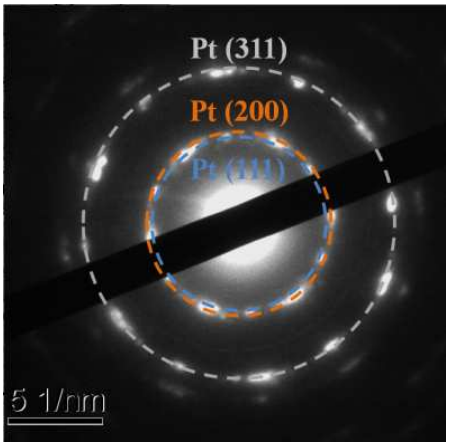


**Figure S3.** SAED pattern of Pt/CNTs-NF.

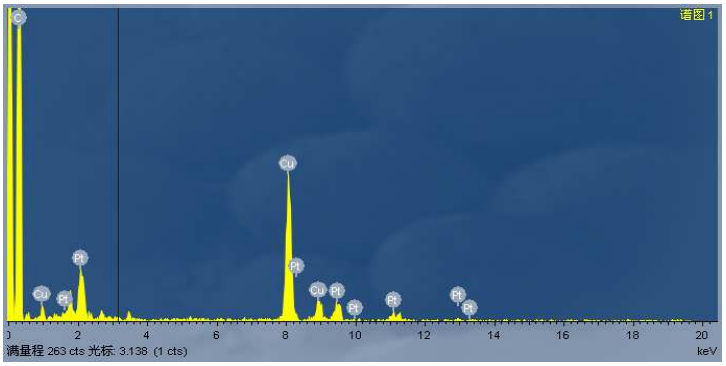


**Figure S4.** EDS pattern of Pt/CNTs-NF.

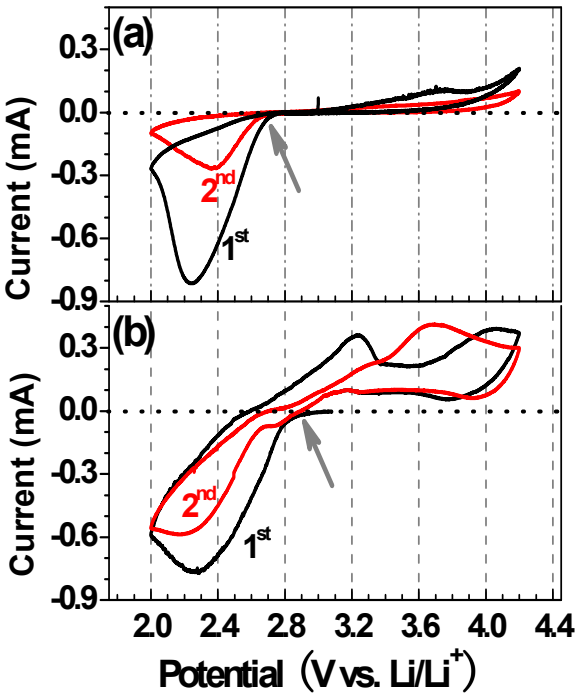


**Figure S5.** CV curves of (a) CNTs-NF electrode and (b) Pt/CNTs-NF electrode.

To explore the application of the CNTs-NF and Pt/CNTs-NF as cathodes in LOBs, the CVs are obtained at a scan rate of 0.2 mV/s. As shown in Figure S5(a), featureless CV curve of CNTs-NF electrode is observed in its OER process, while the Pt/CNTs-NF electrode exhibits an obviously lower OER onset potential and higher OER peak current than CNTs-NF electrode. Meanwhile, in the ORR scan, Pt/CNTs-NF electrode exhibits a slightly higher ORR onset potential in the first cycle as remarked by arrows in Figure S5, and higher ORR peak currents than CNTs-NF electrode in the following cycle. These anodic peaks in ORR process can be attributed to the oxidation of $Li_2O_2$.[1] This result revealed that Pt/CNTs-NF has considerable ORR/OER catalytic activity in non-aqueous LOBs.

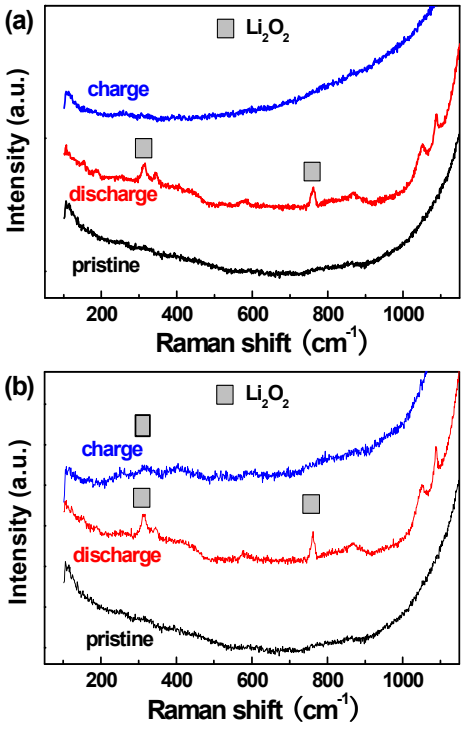


**Figure S6.** Raman patterns for pristine, discharged, and subsequent charged cathodes in Li-$O_2$ batteries using (a) Pt/CNTs-NF and (b) CNTs-NF as electrodes.

As we know, Raman spectroscopy is one of the most useful techniques for measuring $Li_2O_2$ formation during discharge in the Li-Air battery. As in the Raman patterns, $Li_2O_2$ was observed as the major discharge product in the Pt/CNTs-NF and CNTs-NF electrodes.[2] In addition, Raman charged up to a potential of 4.2 V showed no $Li_2O_2$ discharge product for Pt/CNTs-NF electrode, while the CNTs-NF electrode delivered $Li_2O_2$ discharge product. Thus, $Li_2O_2$ is the dominant discharge product for LOBs with a Pt/CNTs-NF electrode used TEGDME-based electrolyte and its formation /decomposition appears to be reversible.

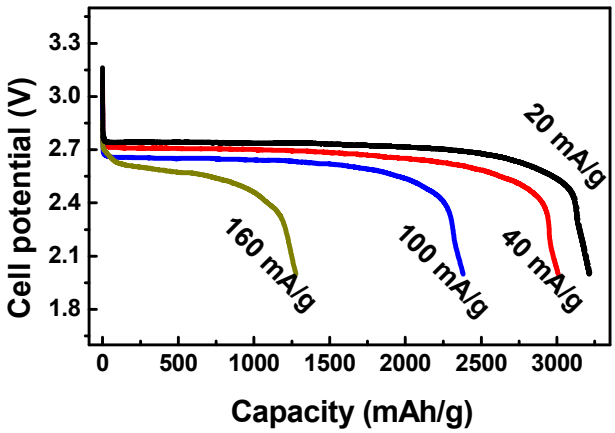


**Figure S7.** Discharge characteristic of the pure CNTs-coating electrodes at various current densities.

**Table S1.** Discharge capacities of the Pt/CNTs-NF, CNTs-NF and pure CNTs-coating electrodes at various current densities.

| Capacities for different electrodes | Current density (mA/g) | | | |
|---|---|---|---|---|
| | 20 | 40 | 100 | 160 |
| Pt/CNTs-NF (mAh/g) | 4050 | 3935 | 3250 | 2815 |
| CNTs-NF (mAh/g) | 4040 | 3822 | 3265 | 2820 |
| CNTs-coating (mAh/g) | 3205 | 3000 | 2375 | 1265 |

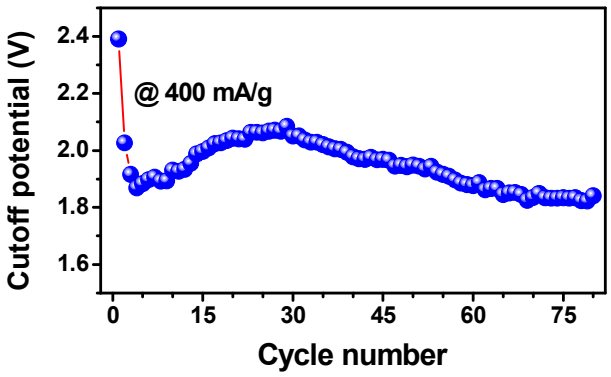


**Figure S8.** Voltage of the terminal discharge with a restriction of the capacity of 1500 mAh/g vs. the cycle number for Li-$O_2$ batteries with Pt/CNTs-NF electrode.

**Table S2.** Electrochemical performance of various Pt/carbon related cathode materials reported in previous works.

| Typical materials | First discharge capacity (mAh/g) /Current density(mA/g) | Cycle number | Last discharge capacity (mAh/g) | Restricting capacity (mAh/g) /Cycle number | Potential difference for ORR/ OER (V) | Refs. |
|---|---|---|---|---|---|---|
| Pt/CNTs-NF | 2900/160 | 4 | 2850 | 1500/80 | 1.1 | this work |
| PtCo/XC-72 carbon | 2578/100 | 10 | 1100 | -- | 1.2 | 3 |
| Pt/GO | 1100/70 | 20 | 980 | -- | 0.7 | 4 |
| Pt/C | 616/70 | 10 | 279 | -- | 1.05 | 5 |
| PtRu/C | -- | -- | -- | 700/42 | -- | 6 |
| Pt/C | 500/240 | 3 | 700 | -- | 1.4 | 7 |
| Pt@MCN | 1500/ (0.02mA/$cm^2$) | 5 | 375 | -- | 0.43 | 8 |
| Pt/C | 870/100 | 3 | 920 | -- | 0.8 | 9 |

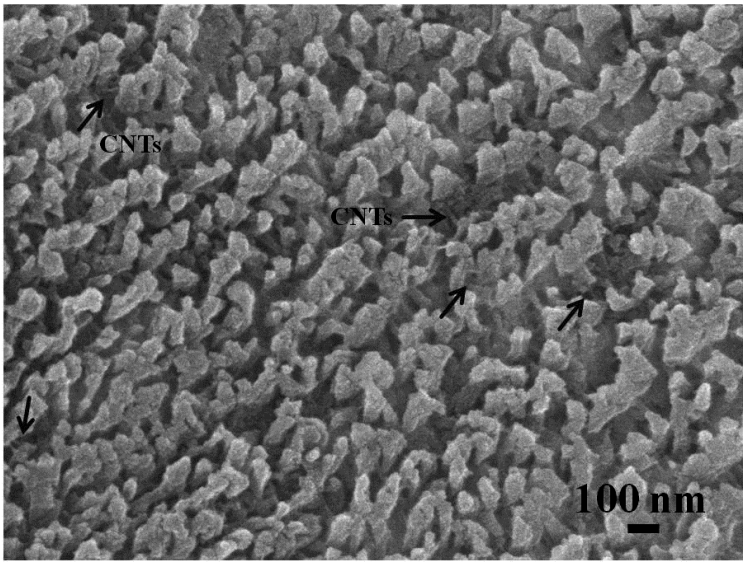


**Figure S9.** SEM and magnified SEM images of the Pt/CNTs-NF electrode after the 21$^{th}$ discharging state at 160 mA/g with a restricting capacity of 800 mAh/g.

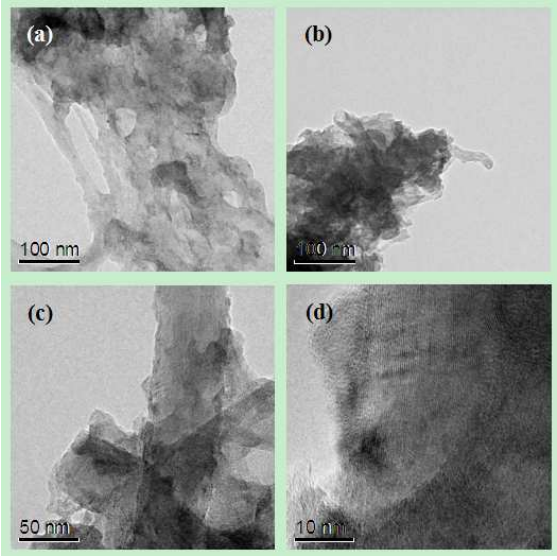

**Figure S10.** Different magnified TEM images for Pt/CNTs-NF cathode after the 21$^{th}$ discharging state at 160 mA/g with a restricting capacity of 800 mAh/g.

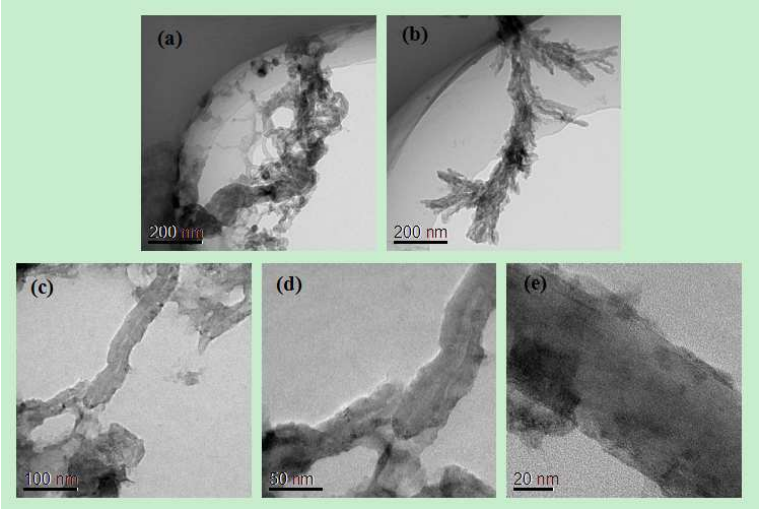


**Figure S11.** Different magnified TEM images for Pt/CNTs-NF cathode after the 86$^{th}$ discharging state at 400 mA/g with a restricting capacity of 1500 mAh/g.

In addition, the corresponding TEM study has been carried out to detect the LOB reaction products. Different magnified TEM images for Pt/CNTs-NF cathode after cycling were shown in the Figures S10~11. For both cathodes, they seemed to be covered by thin products on the CNT surface. Combined with the discussion of XPS and TEM results, the observed close-packed agglomerate shown in Figure 4 in manuscript is believed to be $Li_2O$ and $Li_2O_2$ intermingled with some $Li_2CO_3$.

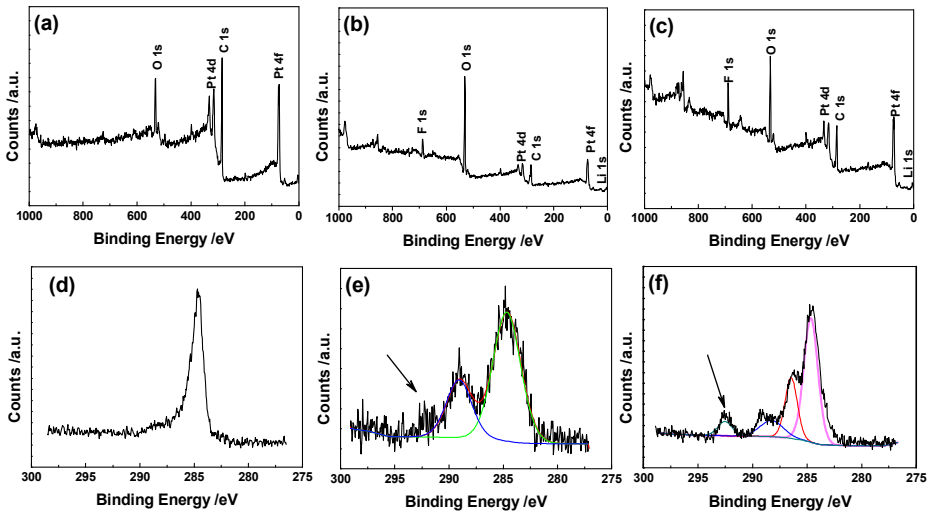


**Figure S12.** Full XPS spectra for Pt/CNTs-NF cathodes for (a) flesh electrode, (b) after the 21$^{th}$ discharging state at 160 mA/g with a restricting capacity of 800 mAh/g, and (c) after the 86$^{th}$ discharging state at 400 mA/g with a restricting capacity of 1500 mAh/g; (d)~(f) the corresponding C 1s XPS spectra for above three cathodes.

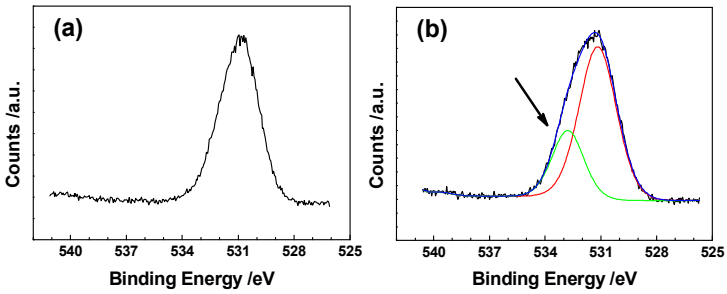


**Figure S13.** The corresponding O 1s XPS spectra for (a) after the 21$^{th}$ discharging state at 160 mA/g with a restricting capacity of 800 mAh/g, and (b) after the 86$^{th}$ discharging state at 400 mA/g with a restricting capacity of 1500 mAh/g.

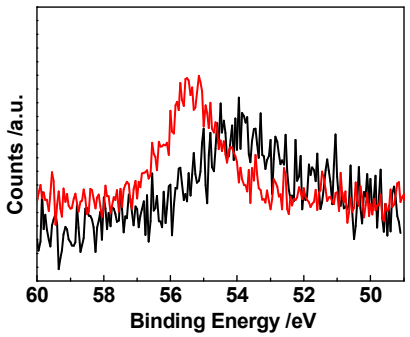


**Figure S14.** The corresponding Li 1s XPS spectra for (a) marked black for after the 21$^{th}$ discharging state at 160 mA/g with a restricting capacity of 800 mAh/g, and (b) marked red for after the 86$^{th}$ discharging state at 400 mA/g with a restricting capacity of 1500 mAh/g.

Combined with the discussion in the manuscript, XPS results are further shown in the following Figures S12-14. As revealed in Figures S12(d) and (e) for the C1s XPS spectra, the signal for C1s at ~292 eV for $Li_2CO_3$ can be found in the both of cathodes. Compared with Figure S12(d), most of them cannot be decomposed in the charged process for the sample after the 86$^{th}$ discharging state at 400 mA/g with a restricting capacity of 1500 mAh/g. As we know, the products of $Li_2CO_3$ can be decomposed when the charged potential is larger than 4.2 V.[1-2] The finding is also supported by the D-C results shown in Figure 3 in manuscript. In addition, in the O 1s XPS spectra shown in Figure S13 presented the components representing $Li_2O_2$ (~531.5 eV), $Li_2O$ (~529.0 eV) and C=O for $CO_3$ (~532.0 eV), [10-13] respectively. It is interesting to note that the peak of ~ 532.0 eV for the $CO_3$ in the products for the sample after the 86$^{th}$ discharging state at 400 mA/g with a restricting capacity of 1500 mAh/g is stronger than that case in Figure S13(a). Meanwhile, Figure S14 shows the absence of $Li_2CO_3$ characteristic signal for Li1s at 55.5 eV in the both of cathodes.[14] Combined with the XPS result shown in Figures S12-14, the observed close-packed agglomerate shown in Fig.4 in manuscript is believed to be $Li_2O$ and $Li_2O_2$ intermingled with some $Li_2CO_3$. As a result, the polarization caused by residual un-decomposed products such

as $Li_2CO_3$, will increase their D-C overpotentials, further leading to fade their cycle performance.

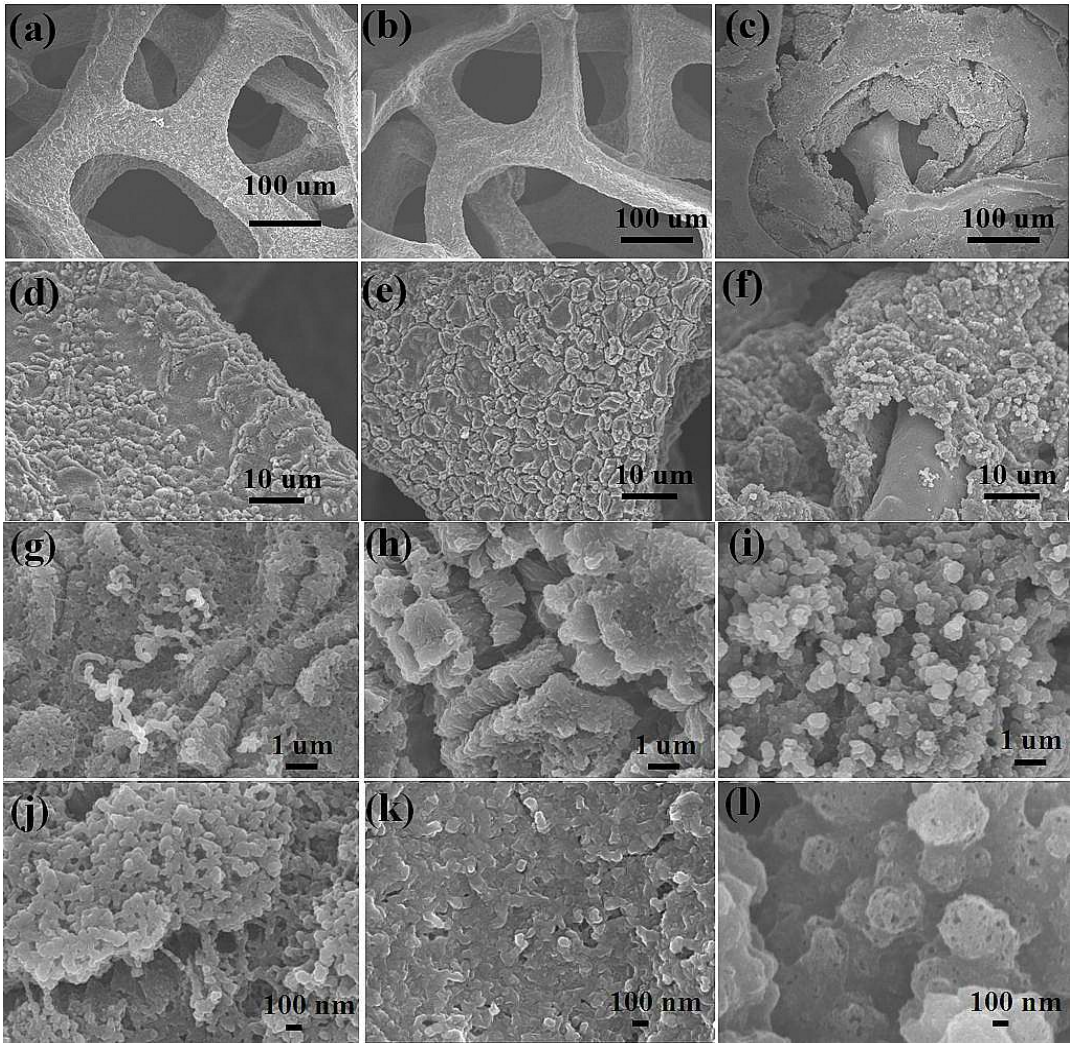


**Figure S15.** SEM and magnified SEM images of the electrodes after long D-C cycles: (a), (d), (g) and (j) for Pt/CNTs-NF electrode; (b), (e), (h) and (k) for CNTs-NF electrode; (c), (f), (i) and (l) for CNTs-coating electrode.

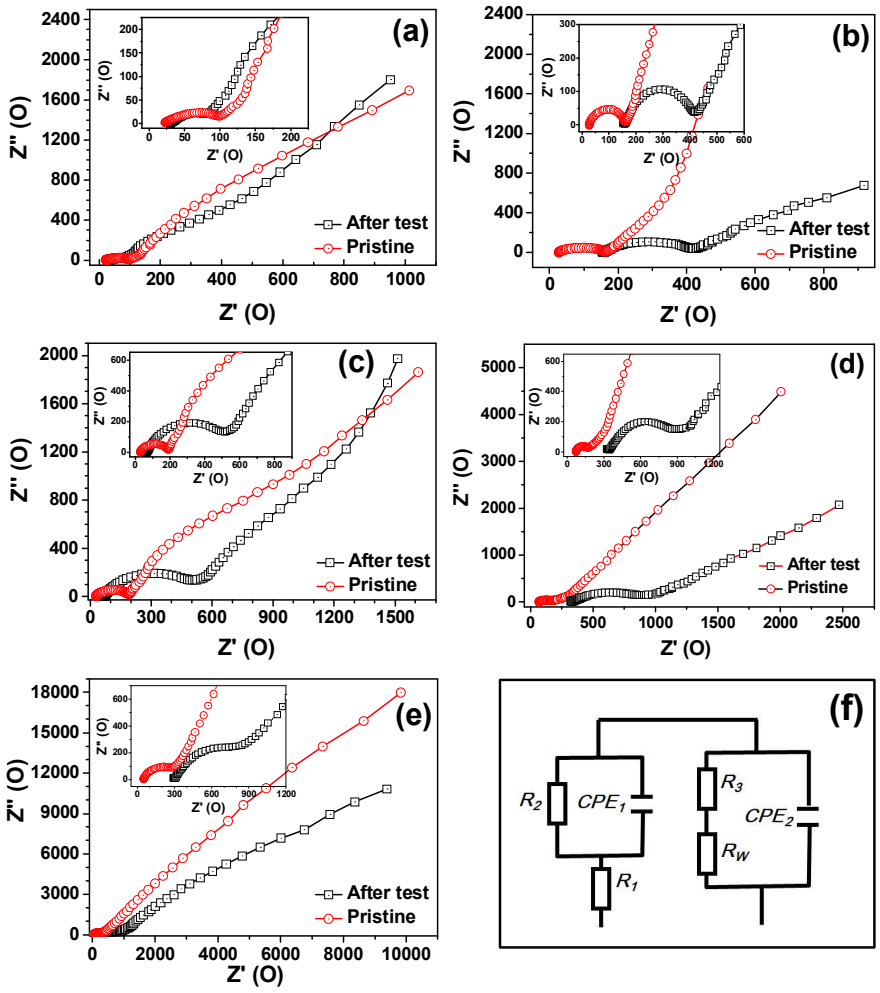


**Figure S16.** Electrochemical impedance spectra (EIS) for LOBs with different D-C stages: (a) Pt/CNTs-NF electrode after 21 cycles at 160 mA/g with curtailing with the capacity to 800 mAh/g; (b) Pt/CNTs-NF electrode after 86 cycles at 400 mA/g with curtailing with the capacity to 1500 mAh/g; (c) Pt/CNTs-NF electrode after long D-C

cycles; (d) CNTs-NF electrode after long D-C cycles; (e) CNTs coating electrode after long D-C cycles; and (f) the corresponding equivalent circuit.

Electrochemical impedance spectroscopy is a highly resolved electroanalytical technique that may provide unique information about the nature of electrode process related to a wide range of time constants.[14] Figure S16 presents EIS profiles of electrochemical impedance spectra for LOBs with different D-C stages and the corresponding equivalent circuit. In the circuit, the high frequency intercept of the semicircle on the real axis was reflected by an ohmic resistance ($R_s$, denoted as $R_1$ in Figure S16(f)), which includes ionic resistance from the separator paper and electrical resistance between the electrode and the current collector. The depressed semicircle at middle frequency was contributed by a parallel combination of charge-transfer resistance ($R_{ct}$), corresponding to the kinetic reaction at the air electrode surface, which can be divided into $R_2$ and $R_3$ in Figure S16(f). The linear spike at low frequency could be described by a finite length Warbury element $R_W$.[15]

## REFERENCES AND NOTES


1. Zhang, K.; Zhang, L.; Chen, X.; He, X.; Wang, X.; Dong, S.; Han, P.; Zhang, C.; Wang, S.; Gu, L.; Cui, G. Mesoporous Cobalt Molybdenum Nitride: A Highly Active Bifunctional Electrocatalyst and Its Application in Lithium–$O_2$ Batteries *J Phys. Chem. C* 2013, 117, 858-865.

2. McCloskey, B. D.; Bethune, D. S.; Shelby, R. M.; Girishkumar, G.; Luntz, A. C. Solvents' Critical Role in Nonaqueous Lithium–Oxygen Battery Electrochemistry *J Phys. Chem. Lett.* 2011, 2, 1161-1166.

3. Su, D.; Kim, H.-S.; Kim, W.-S.; Wang, G., A Study of $Pt_xCo_y$ Alloy Nanoparticles as Cathode Catalysts for Lithium-Air Batteries with Improved Catalytic Activity *J Power Sources* 2013**,** 244, 488-493.

4. Wang, L.; Ara, M.; Wadumesthrige, K.; Salley, S.; Ng, K. Y. S. Graphene Nanosheet Supported Bifunctional Catalyst for High Cycle Life Li-Air Batteries *J Power Sources* 2013, 234, 8-15.

5. Cheng, H.; Scott, K., Selection of Oxygen Reduction Catalysts for Rechargeable Lithium-Air Batteries-Metal or Oxide? *Appl. Catal. B: Environ.* 2011, 108-109, 140-151.

6. Ko, B. K.; Kim, M. K.; Kim, S. H.; Lee, M. A.; Shim, S. E.; Baeck, S.-H., Synthesis and Electrocatalytic Properties of Various Metals Supported on Carbon for Lithium-Air Battery *J Mole. Catal. A: Chem.* 2013, 379, 9-14.

7. Yin, J.; Fang, B.; Luo, J.; Wanjala, B.; Mott, D.; Loukrakpam, R.; Ng, M. S.; Li, Z.; Hong, J.; Whittingham, M. S.; Zhong, C.-J., Nanoscale Alloying Effect of Gold–Platinum Nanoparticles as Cathode Catalysts on the performance of A Rechargeable Lithium–Oxygen Battery. *Nanotechnology* 2012, 23 (30), 305404.

8. Lu, Y.; Wen, Z.; Jin, J.; Cui, Y.; Wu, M.; Sun, S., Mesoporous Carbon Nitride Loaded with Pt Nanoparticles as A Bifunctional Air Electrode for Rechargeable Lithium-Air Battery *J Solid State Electrochem.* 2012, 16 (5), 1863-1868.

9. Lu, Y.-C.; Xu, Z.; Gasteiger, H. A.; Chen, S.; Hamad-Schifferli, K.; Shao-Horn, Y. Platinum−Gold Nanoparticles: A Highly Active Bifunctional Electrocatalyst for Rechargeable Lithium−Air Batteries *J Am. Chem. Soc.* 2010, 132, 12170-12171.

10. Lu, Y.-C.; Crumlin, E. J.; Carney, T. J.; Baggetto, L.; Veith, G. M.; Dudney, N. J.; Liu, Z.; Shao-Horn, Y., Influence of Hydrocarbon and $CO_2$ on the Reversibility of Li-O2Chemistry UsingIn SituAmbient Pressure X-ray Photoelectron Spectroscopy *J Phys. Chem. C* 2013, 117 (49), 25948-25954.

11. Li, F.; Tang, D.-M.; Chen, Y.; Golberg, D.; Kitaura, H.; Zhang, T.; Yamada, A.; Zhou, H., Ru/ITO: A Carbon-Free Cathode for Nonaqueous Li-O2 Battery *Nano Lett.* 2013, 13 (10), 4702-4707.

12. Ottakam Thotiyl, M. M.; Freunberger, S. A.; Peng, Z.; Bruce, P. G. The Carbon Electrode in Nonaqueous Li-$O_2$ Cells *J. Am. Chem. Soc.* 2013, 135, 494-500.

13. S. A. Freunberger, Y. Chen, N. E. Drewett, L. J. Hardwick, F. Bardé and P. G. Bruce, *Angewandte Chemie International Edition*, 2011, **50**, 8609.

14. Kitaura, H.; Zhou, H. Electrochemical Performance of Solid-State Lithium-Air Batteries Using Carbon Nanotube Catalyst in the Air Electrode *Adv. Ener. Mater.* 2012, 2, 889-894.

15. Kichambare, P.; Kumar, J.; Rodrigues, S.; Kumar, B. Electrochemical Performance of Highly Mesoporous Nitrogen Doped Carbon Cathode in Lithium–Oxygen Batteries *J Power Sources* 2011, 196, 3310-3316.